⌘ *Author's Choice*

Structure of the Tandem MA-3 Region of Pdcd4 Protein and Characterization of Its Interactions with eIF4A and eIF4G
MOLECULAR MECHANISMS OF A TUMOR SUPPRESSOR[*][S]

Lorna C. Waters[‡1]**, Sarah L. Strong**[‡]**, Eva Ferlemann**[§]**, Ojore Oka**[‡]**, Frederick W. Muskett**[‡]**, Vaclav Veverka**[‡]**,
Sreemoti Banerjee**[‡]**, Thore Schmedt**[§]**, Alistair J. Henry**[¶]**, Karl-Heinz Klempnauer**[§]**, and Mark D. Carr**[‡2]

From the [‡]*Department of Biochemistry, Henry Wellcome Building, University of Leicester, Lancaster Road, Leicester LE1 9HN, United Kingdom, the* [§]*Institut für Biochemie, Westfälische-Wilhelms-Universität Münster, Wilhelm-Klemm-Str. 2, D-48149 Münster, Germany, and* [¶]*Research and Development, UCB-Celltech, Slough SL1 3WE, United Kingdom*

One of the key regulatory points of translation initiation is recruitment of the 43S preinitiation complex to the 5′ mRNA cap by the eIF4F complex (eIF4A, eIF4E, and eIF4G). The tumor suppressor protein Pdcd4 has been shown to inhibit cap-dependent translation by interacting tightly with the RNA helicase eIF4A via its tandem MA-3 domains. The NMR studies reported here reveal a fairly extensive and well defined interface between the two MA-3 domains in solution, which appears to be stabilized by a network of interdomain salt bridges and hydrogen bonds, and reveals a unique orientation of the two domains. Characterization of the stoichiometry of the Pdcd4-eIF4A complex suggests that under physiological conditions Pdcd4 binds to a single molecule of eIF4A, which involves contacts with both Pdcd4 MA-3 domains. We also show that contacts mediated by a conserved acidic patch on the middle MA-3 domain of Pdcd4 are essential for forming a tight complex with eIF4A *in* vivo, whereas the equivalent region of the C-terminal MA-3 domain appears to have no role in complex formation *in vivo*. The formation of a 1:1 eIF4A-Pdcd4 complex in solution is consistent with the reported presence *in vivo* of only one molecule of eIF4A in the eIF4F complex. Pdcd4 has also been reported to interact directly with the middle region of eIF4G, however, we were unable to obtain any evidence for even a weak, transient direct interaction.

The highly conserved eukaryotic protein Pdcd4[3] (programmed cell death protein 4) was initially discovered in a screen for genes activated during apoptosis (1) and then subsequently identified as a tumor suppressor in studies of a mouse keratinocyte model of tumor promotion (2). The role of Pdcd4 as a tumor suppressor protein has been confirmed by several additional studies, for example, Pdcd4 has been shown to suppress tumor development in a mouse model of skin carcinogenesis (3), and Pdcd4 knock-out mice were found to develop spontaneous lymphomas (4). In addition, decreased expression of Pdcd4 has been strongly implicated in the development and progression of many human cancers, including lung, breast, colon, renal, and liver (5–11). Pdcd4 has also been shown to play an essential role in cellular responses to DNA damage (12, 13). The molecular mechanisms by which Pdcd4 functions as a tumor suppressor are not entirely clear, however, Pdcd4 has been shown to play critical roles in the regulation of both transcription and translation, mediated via specific protein-protein and protein-RNA interactions (14–19).

Pdcd4 is composed of three regions: an unstructured N-terminal RNA-binding region (16, 17) and two interacting MA-3 domains (MA-3$_M$ and MA-3$_C$) (Fig. 1*a*) (20–23). To date, the majority of the molecular and structural studies have focused on the interaction between the two MA-3 domains of Pdcd4 and the eukaryotic translation initiation factor 4A (eIF4A) (Fig. 1*b*).

eIF4A is an RNA helicase that catalyzes the unwinding of secondary structure in the 5′ untranslated region (UTR) of mRNA, allowing the recruitment of the 43S small ribosomal subunit to the 5′ cap and subsequent scanning (reviewed in Refs. 24 and 25). Its inherent helicase activity is strongly stimulated by binding to the scaffold protein eIF4G to form part of the eIF4F complex (eIF4A, eIF4G, and eIF4E), or when bound to RNA-binding proteins eIF4B or eIF4H (26–29). The recruitment of eIF4A to the eIF4F cap-binding complex is mediated by two HEAT repeat domains within eIF4G: the mIF4G domain and the C-terminal MA-3 domain (Fig. 1*c*). The mIF4G domain is located within the middle third of eIF4G (eIF4Gm), which has also been implicated in binding to eIF3 and mRNA (30–33). The interaction of eIF4A with eIF4Gm is sufficient for cap-dependent translation (34) and it is believed that this interaction helps tether eIF4A to the RNA, as well as helping to stabilize the interdomain orientation of the N- and C-terminal domains of eIF4A (35–37). The eIF4G MA-3 domain is homologous to the MA-3 domains of Pdcd4 and has been shown to play a modu-

[3] The abbreviations used are: Pdcd4, programmed cell death protein 4; HEAT, Huntingtin, elongation factor 3, A subunit of protein phosphatase 2A, target of rapamycin; mIF4G, middle of eIF4G; eIF4Gm, middle third of eIF4G; MA-3$_C$, C-terminal MA-3 domain; MA-3$_M$, middle MA-3 domain; MA-3$_{M-C}$, tandem MA-3 region; RDC, residual dipolar coupling; TROSY, transverse relaxation optimized spectroscopy; HSQC, heteronuclear single quantum coherence.
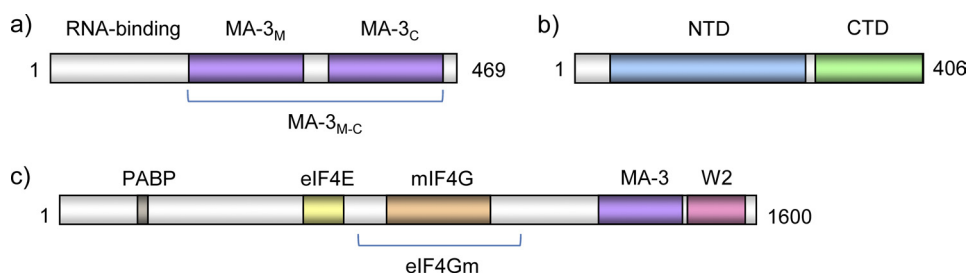
FIGURE 1. **Schematic diagram of the functional regions of Pdcd4 and translation initiation factors eIF4A and eIF4G.** *Panel a,* shows a schematic representation of the functional regions of mouse Pdcd4. The RNA-binding region (residues 1–157), middle MA-3 domain (MA-3$_M$) (157–305), C-terminal MA-3 domain (MA-3$_C$) (319–449), and tandem MA-3 region (MA-3$_{M-C}$) (157–449) are indicated. Similarly, *panels b* and *c* show schematic diagrams of mouse eIF4AI and eIF4GI, respectively. The N- (residues 35–235) and C-terminal (247–406) domains of eIF4A, and the PABP-binding region (165–210), eIF4E-binding region (557–681), mIF4G (752–993), MA-3 (1235–1426), and W2 (1437–1565) domains of eIF4G are highlighted. In addition, the middle third region of eIF4G (eIF4Gm) is also indicated (672–1065).

latory role on translation (32). The MA-3 domain competes with RNA for binding to eIF4A and is believed to stabilize the inactive conformation of eIF4A (22, 35). Pdcd4 has been shown to compete with RNA and the eIF4G MA-3 domain for binding to eIF4A, with complex formation resulting in the inhibition of cap-dependent translation (14, 15, 21, 22, 38). In addition, Pdcd4 has been reported to interact with eIF4Gm in both the presence and absence of eIF4A (14, 39).

The structures of both the isolated C-terminal (MA-3$_C$) and middle (MA-3$_M$) MA-3 domains of Pdcd4 have been solved and are shown to be composed of three and four layers of atypical HEAT repeats, respectively, as shown in Fig. 2, *c* and *f* (20, 22, 38). More recently, crystal structures of the entire tandem MA-3 region (MA-3$_{M-C}$), as well as the structure of the Pdcd4 MA-3$_{M-C}$ region in complex with eIF4A have been reported (21, 40). Surprisingly, the complex structures revealed two molecules of eIF4A bound to a single molecule of Pdcd4 via distinct interaction modes.

In this communication we report the overall architecture of the tandem MA-3$_{M-C}$ region in solution, which is very similar to the recently described crystal structure, but also reveals the positioning of the flexible linker between the two MA-3 domains. A series of complementary experiments also provide compelling evidence that at near physiological conditions, Pdcd4 binds only one molecule of eIF4A. In contrast to previous reports we were unable to detect any evidence of a direct interaction between Pdcd4 and eIF4Gm.

EXPERIMENTAL PROCEDURES

Protein Expression and Purification—Uniformly ^{15}N- and ^{15}N/^{13}C-labeled samples of mouse Pdcd4 MA-3$_M$ (residues 157–318), Pdcd4 MA-3$_C$ (residues 319–449), Pdcd4 MA-3$_{M-C}$ (residues 157–449), and full-length Pdcd4 were prepared from pGex-6P-2-based *Escherichia coli* expression vectors as described previously (41, 42). In addition, a ^{15}N/^{2}H sample of MA-3$_{M-C}$ was prepared from cells grown in fully deuterated minimal media. The N-terminal histidine-tagged full-length mouse eIF4AI, eIF4GmII (residues 674–1039), and the eIF4GI mIF4G domain (residues 745–1013) were prepared from modified pET-based *E. coli* expression vectors (Protex, University of Leicester) essentially as described previously (20, 43, 44).

Pull-down Assays—Pull-down assays between either GST-full-length Pdcd4 or GST-MA-3$_{M-C}$ fusion proteins and eIF4A were carried as follows. Initially, a 0.5-ml sample of 7 μM GST

full-length Pdcd4 or GST-MA-3$_{M-C}$ was loaded onto a pre-equilibrated 0.5-ml glutathione-agarose column and washed with 5 column volumes of binding buffer (20 mM Tris, 100 mM sodium chloride, 2 mM DTT, and 1 mM EDTA buffer, pH 7.4). A 0.5-ml sample of 7, 21, or 35 μM eIF4A was then loaded onto the column and washed with 5 column volumes of binding buffer to remove unbound proteins. Bound proteins were eluted by the addition of binding buffer containing 10 mM reduced glutathione and the eluted fractions were analyzed by SDS-PAGE. Similar pull-down assays were performed between GST full-length Pdcd4 or GST-MA-3$_{M-C}$ fusion proteins and either eIF4Gm or the mIF4G domain, but using a binding buffer of 20 mM Tris, 150 mM sodium chloride, 2 mM DTT and 1 mM EDTA, pH 7.4.

Analytical Gel Filtration—The binding ratio of MA-3$_{M-C}$ and eIF4A was investigated by analytical gel filtration on a Superdex 200 10/300 column (GE Healthcare). Initially, 7-μm samples (0.5 ml) of either the MA-3$_{M-C}$ or eIF4A in isolation were loaded onto the column, which had been pre-equilibrated in 25 mM sodium phosphate, 125 mM sodium chloride, 5 mM DTT, and 50 μM EDTA buffer, pH 7. Samples of MA-3$_{M-C}$ and eIF4A were premixed to give a 0.5-ml sample of 7 μM MA-3$_{M-C}$ and 7, 14, or 35 μM eIF4A. The samples were allowed to equilibrate for 30 min at room temperature prior to being loaded onto the column. The column was calibrated using a range of molecular mass protein standards (6.5, 13.7, 29, 43, 75, 158, 440, and 669 kDa) supplied by GE Healthcare. Elution fractions were analyzed by SDS-PAGE, with the relative staining intensity of Coomassie-stained bands determined using the program TINA (Isotopenmessgerate GmbH).

Biacore—The affinity of the MA-3$_{M-C}$-eIF4A interaction was determined on a Biacore 3000 biosensor. Mouse anti-GST monoclonal antibody was coupled to a CM5 sensor chip by amine coupling according to the manufacturer's instructions. Typically, coupling densities of 12,000 response units were achieved. A control flow cell was prepared without the anti-GST antibody. All kinetic experiments were performed at 30 μl/min in either high salt HBS buffer (10 mM Hepes, 150 mM sodium chloride, 3 mM EDTA, 0.005% P20 (v/v), pH 7.4) or low salt HBS buffer (10 mM Hepes, 50 mM sodium chloride, 3 mM EDTA, 0.005% P20 (v/v), pH 7.4). The chip was regenerated between assay cycles with two 2-min pulses of 10 mM glycine HCl, pH 2.2. GST-MA-3$_{M-C}$ fusion protein was diluted to 10 μg/ml in the appropriate HBS buffer and captured onto the

anti-GST surface. Capture levels were limited to 200 response units to reduce the possibility of mass transport limited binding in the kinetic experiments (45, 46). Recombinant eIF4A was titered from 10 μM and binding levels of eIF4A at equilibrium were monitored and normalized with respect to the GST-MA-3$_{M-C}$ capture level. The affinity of the interaction was determined by non-linear regression analysis of the normalized binding curves (45, 46). For interactions measured in the low salt HBS buffer, the sensorgrams were double referenced and fitted to a 1:1 model of binding using the BiaEvaluation 3.2 software.

In Vivo GFP-Trap Experiments—QT6 fibroblast cells were transfected by calcium-phosphate co-precipitation with the following plasmids: pCDNA3-eIF4AI-FLAG (encoding FLAG-tagged full-length mouse eIF4AI), pEYFP-C1, pEYPF-C1-hPdcd4 (encoding YFP fused to full-length human Pdcd4), pEYFP-C1-hPdcd4-E249A/D253A, or pEYFP-C1-hPdcd4-D414A/D418A encoding YFP fused to full-length human Pdcd4 harboring the indicated amino acid replacements. Cells were lysed 24 h post-transfection in ELB buffer (500 μl/10-cm dish; ELB buffer: 120 mM sodium chloride, 50 mM Tris/HCl, pH 7.4, 20 mM sodium fluoride, 1 mM EDTA, 6 mM EGTA, 15 mM sodium pyrophosphate, 1 mM PMSF, 0.5% Nonidet P-40, 1 μg/ml of aprotinin, 0.2 μg/ml of leupeptin, 1 μg/ml of pepstatin) and centrifuged for 20 min at 14,000 $\times$ g. 10% of the supernatant was retained for input control, the remaining 90% was incubated with GFP-trap beads (Chromotec, München) for 3 h at 4 °C. Beads were washed 3 times with ELB buffer, boiled in SDS sample buffer, and analyzed together with the input samples by SDS-PAGE and Western blotting. Proteins were detected with anti-FLAG or anti-YFP antibodies.

NMR Spectroscopy—NMR spectra of Pdcd4 MA-3$_M$, MA-3$_C$, and MA-3$_{M-C}$, both in isolation and in complex with either eIF4A or eIF4Gm, were recorded as described under supplemental "Methods". Differences between the backbone amide and carbonyl chemical shifts of the individual MA-3$_M$ and MA-3$_C$ domains and the entire MA-3$_{M-C}$ region were used to identify the intramolecular interface between the MA-3 domains as described under supplemental "Methods".

Determination of the Pdcd4 MA-3$_{M-C}$ Structure Using NMR Restraint-driven Docking—The structure of the MA-3$_{M-C}$ region was determined by NMR restraint-driven docking using the program HADDOCK essentially as described by the authors (47). Further details are provided under supplemental "Methods".

RESULTS

Mapping of the Pdcd4 MA-3$_M$/MA-3$_C$ Intra-molecular Interface—The positions of NMR signals from the backbone carbonyl and amide groups in proteins are highly sensitive to changes in their local environment, and shifts in these signals were used to localize the intra-molecular interface between the Pdcd4 MA-3 domains. Comparison of NMR signals in HNCO spectra of the individual MA-3 domains and the entire MA-3$_{M-C}$ region allowed combined backbone amide and/or carbonyl shift values to be determined for nearly all the residues in the MA-3$_{M-C}$ region, which are summarized in the histogram shown in Fig. 2a. Examination of the histogram clearly

identifies 22 residues (Lys[212], His[215], Arg[216], Glu[217], Met[218], Gln[259], Leu[260], Val[261], Phe[264], Arg[267], Met[304], Lys[309], Val[314], Gly[316], Ser[317], Gly[318], Gln[322], Pro[323], Val[324], Met[333], Tyr[338], and Pro[413]) in MA-3$_{M-C}$ whose backbone amide/carbonyl signals undergo large combined chemical shift changes (>0.05 ppm) relative to the position of the signals observed in the spectra of the isolated MA-3 domains. No shift data could be obtained for a small number of residues (Ala[213], Asn[325], Val[328], Lys[329], Glu[330], Val[356], Ile[412], Ile[415], Asn[416], Leu[417], Asp[418], Val[419], Pro[420], His[421], Pro[448], and Ser[449]), the majority of which are located in the conformationally hetergeneous loop located between helices α5 and α6 of MA-3$_C$ (20).

The majority of the perturbed residues clearly map to two relatively large, contiguous surfaces, primarily involving solvent-exposed residues located in helices α4 and α6 of MA-3$_M$ and helices α1 and α2 of MA-3$_C$ as highlighted in Fig. 2. In addition, a small patch of affected residues are located in and around the loop between helices α5 and α6 of MA-3$_C$. This negatively charged region of MA-3$_C$ forms a major part of the eIF4A binding site for the isolated domain and has previously been shown to be poorly defined in solution (20). It seems very unlikely that this region forms part of the interface between the two MA-3 domains, which suggests that signals from residues in this highly charged, semi-flexible region are either very sensitive to small changes in ionic strength or pH, or that the chemical changes seen are a result of secondary effects on the structure, such as stabilization of the loop region, caused by the interaction between the two MA-3 domains.

NMR Restraint-driven Docking of Pdcd4 MA-3$_M$ and MA-3$_C$—The docking calculations were primarily driven by knowledge of the interaction surfaces on the two domains obtained from backbone amide/carbonyl chemical shift perturbations and by information on the relative orientation of the two domains from backbone amide residual dipolar couplings (RDCs). Analysis of the chemical shift perturbation data (Fig. 2a) resulted in 19 active and 14 passive residues being selected for MA-3$_M$, and 12 active and 14 passive residues being selected for MA-3$_C$. Backbone amide RDC values obtained for 165 residues (92 from MA-3$_M$ and 73 from MA-3$_C$) of MA-3$_{M-C}$ were used as restraints defining the orientation of the domains (supplemental Fig. S1a). RDC values from residues in poorly defined/flexible regions, or those whose NMR signals could not be accurately assigned due to overlap in the HNCO spectra, were excluded from the docking calculations. Backbone torsion angle restraints obtained from TALOS (92 for MA-3$_M$ and 73 for MA-3$_C$), and one distance restraint used to tether the C termini of MA-3$_M$ and the N termini of MA-3$_C$ were also included in the docking calculations.

The docking process produced one main cluster for the Pdcd4 MA-3$_{M-C}$ region (overall backbone root mean square deviations for residues 158–305 and 326–446 of 1.38 Å), which contained 195 of the 200 calculated structures. For further analysis we reduced the family of structures to include all those up to the point at which the backbone root mean square deviations (residues 158–305 and 326–446) started to diverge significantly from the structure with the lowest HADDOCK score. The resulting family contained 73 converged structures with root mean square deviation values to the mean structure for
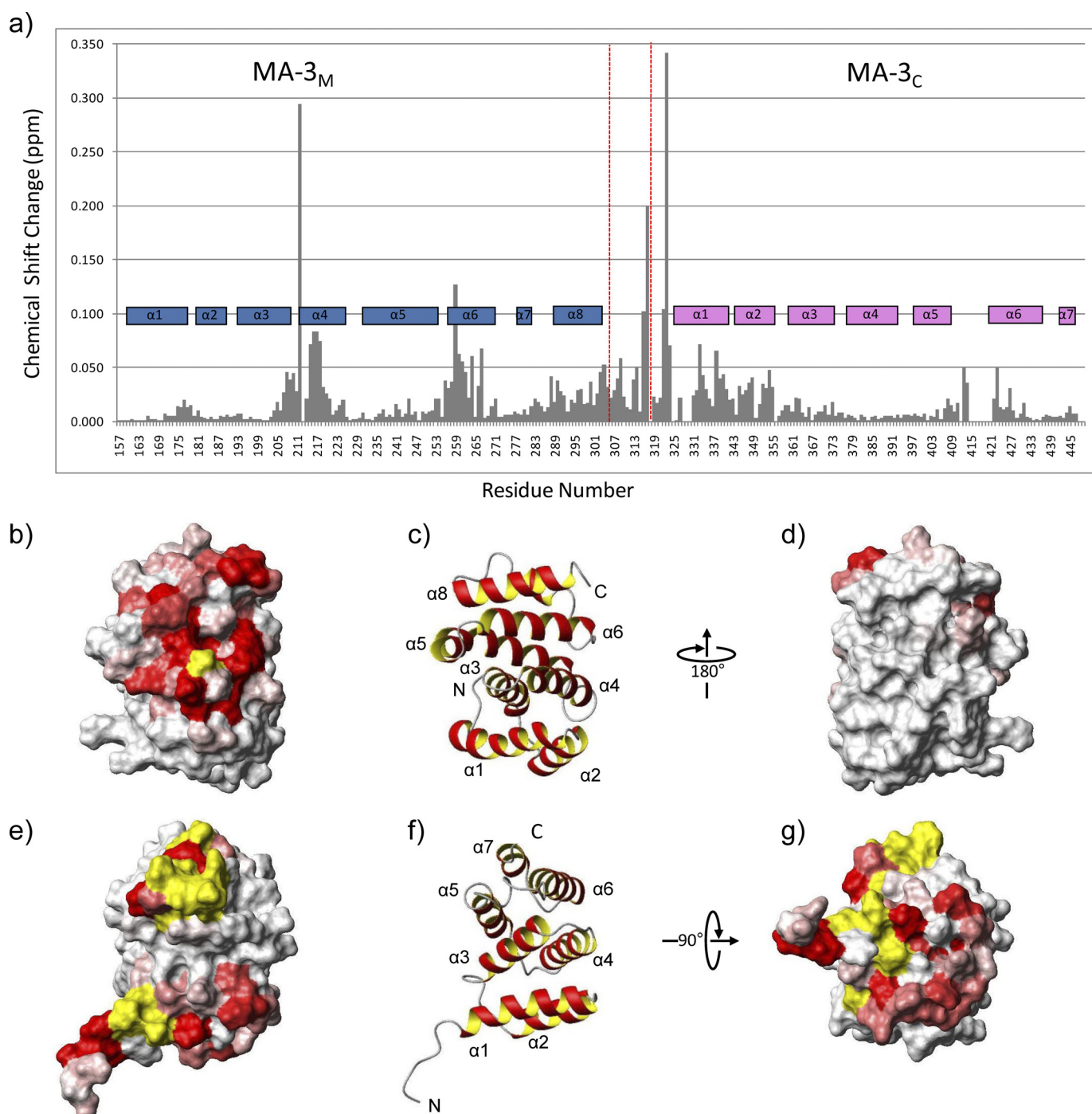
FIGURE 2. **Location of the interface between the Pdcd4 MA-3$_M$ and MA-3$_C$ domains.** The histogram shown in *panel a* summarizes the combined differences between the backbone amide and carbonyl chemical shifts of the individual Pdcd4 MA-3$_M$ and MA-3$_C$ domains and the entire MA-3$_{M-C}$ region. The boundaries between the MA-3 domains are marked with *red dashed lines*. To compensate for the increased chemical shift range of nitrogen and carbon compared with proton, the overall change was calculated by taking the absolute value of: $(\Delta^1 HN + (\Delta^{15}N \times 0.2) + (\Delta^{13}CO \times 0.35))/3$. The position of the helices in MA-3$_M$ and MA-3$_C$ are highlighted on the histogram in *blue* and *pink*, respectively. *Panels b* and *d* show surface views of MA-3$_M$ (PDB code 2RG8 (22)) in which residues are colored according to the perturbation of the backbone amide and carbonyl signals induced by their interaction with MA-3$_C$. Residues that showed a minimal shift change of less than 0.015 ppm are shown in *white*, over 0.050 ppm in *red*, and between 0.015 and 0.050 ppm are colored according to the magnitude of the shift on a linear gradient between *white* and *red*. Residues for which no data were obtained are shown in *yellow*. The structure in *panel d* is rotated by 180° about the *y* axis from the view shown in *panel b*. *Panel c* shows a ribbon representation of the backbone topology of MA-3$_M$ shown in the same orientation as *panel b*. Residues 306–318, most of which were also significantly perturbed are absent from this structure. *Panels e* and *g* show surface views of Pdcd4 MA-3$_C$ (PDB code 2HM8 (20)) in which residues are colored according to the perturbation of the backbone amide and carbonyl signals induced by their interaction with MA-3$_M$, as described for *panels b* and *d*. The structure in *panel g* is rotated by −90° about the *x* axis from the view shown in *panel e*. *Panel f* shows a ribbon representation of the backbone topology of MA-3$_C$ shown in the same orientation as *panel e*. The structures of MA-3$_M$ shown in *panels b* and *c* are rotated by 45° about the *y* axis from the views of MA-3$_C$ shown in *panels e* and *f*.
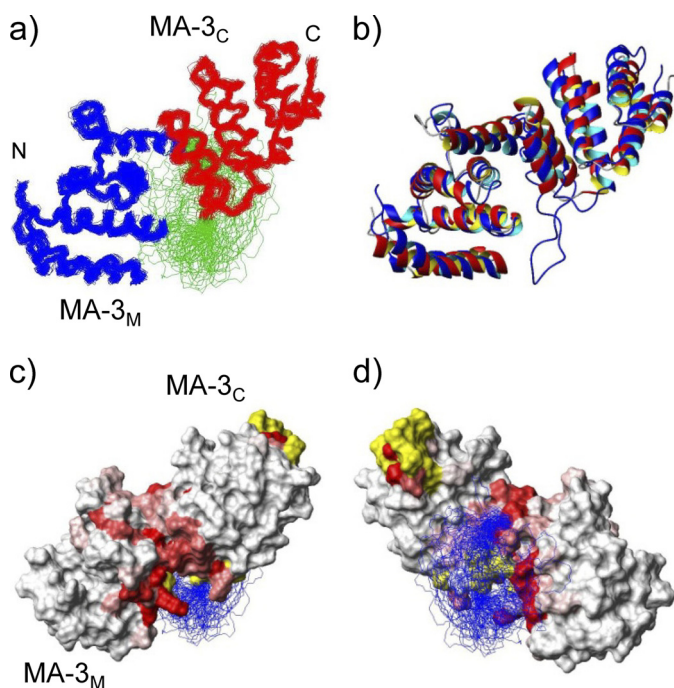
FIGURE 3. **Solution structure of the Pdcd4 MA-3$_{M-C}$ region.** *Panel a* shows a superposition of the protein backbone (residues Pro[158]-Ser[305] and His[326]-Leu[446]) for the family of 73 satisfactorily converged structures obtained from HADDOCK. For clarity MA-3$_M$ (residues Gly[156]-Ser[305]) is shown in *blue*, MA-3$_C$ (Asn[325]-Ser[449]) in *red*, and the unstructured linker region (Lys[306]-Val[324]) in *green*. *Panel b* shows an overlay of the ribbon representation of the backbone topology of the Pdcd4 MA-3$_{M-C}$ crystal structure (PDB code 3EIJ (21)) (shown in *red*) and the lowest energy structure obtained from HADDOCK (shown in *blue*), which was obtained by superimposing the backbone atoms of residues Pro[158]-Lys[283], Asp[287]-Ser[305], and His[326]-Leu[446]. Residues Gly[234]-Val[286] and Gly[307]-Ser[323] are absent from the crystal structure. *Panels c and d* show surface views of the lowest energy MA-3$_{M-C}$ solution structure derived from HADDOCK. The residues are colored according to the perturbation of the backbone amide and carbonyl signals induced by the interaction between the MA-3 domains as described in the legend to Fig. 2. The backbone traces of the unstructured linker region (residues Lys[306]-Val[324]) from the family of 73 converged structures are shown in *blue*. The structure shown in *panel c* is shown in the same orientation as the structures shown in *panel a*, whereas the structure shown in *panel d* is rotated by 180° about the *y* axis from the view shown in *panel a*.

both the backbone and all heavy atoms of 0.68 ± 0.10 and 0.96 ± 0.11 Å, respectively (for residues 158–305 and 326–446) (Fig. 3*a*). The final family of structures have been deposited in the Protein Data Bank (Protein Data Bank code 2KZT).

The final set of converged MA-3$_{M-C}$ structures is consistent with the NMR-derived constraints used for the docking, with few significant or consistent violations. The amide proton line widths of the TROSY-HNCO peaks used to acquire the backbone RDC data were approximately 30 Hz, which is consistent with an uncertainty of approximately ±2.0 Hz. Analysis of the converged structures revealed that an average of only 20.4 ± 10.0 of the total 165 backbone RDC restraints (12.4%) were violated by over 2 Hz. In the case of the TALOS restraints, only 21 of the 330 (165 pairs of φ and ψ angle ranges) angle restraints were violated in over 25% of the structures. The vast majority of apparent inconsistencies are a result of the very narrow angle ranges obtained from TALOS. The remaining violated angle restraints probably reflect the known 2% error rate for TALOS predictions (48).

The crystal and docked-solution Pdcd4 MA-3$_{M-C}$ structures contain very similar secondary and tertiary structures, which is

clearly evident from the superposition of the protein backbones shown in Fig. 3*b* (superimposed on residues 158–283, 287–305, and 326–446) and is reflected in a relatively low root mean square deviation value for the backbone atoms of 2.82 ± 0.15 Å. The positions of the helices within the sequence are essentially identical apart from the crystal structure contains an additional helical turn at the N-terminal end of MA-3$_M$ α1 and there is an additional helical region in the solution structure (MA-3$_M$ α7: residues Tyr[278]-Ser[281]). In the crystal structure this region is composed of a series of bends and turns, however, it should be noted that the B-factors for this region are somewhat higher than average (for Cα > mean ± 1.5 S.D.). Comparison of the crystal and solution structures also reveals subtle changes in the relative positioning of the two MA-3 domains, with MA-3$_C$ being positioned slightly closer to the N-terminal end of MA-3$_M$ helices α6 and α8 in the solution structures. Despite this difference in orientation, the interdomain interface in both the crystal and solution structures is stabilized by a very similar set of electrostatic interactions primarily between: Arg[256]-Glu[346], Arg[256]-Glu[353], Lys[297]-Glu[337], and Lys[297]-Glu[346]. In addition, two interdomain hydrogen bonds, involving residues Arg[256]-Glu[353] and Lys[297]-Glu[346], were observed in over 60% of the converged solution structures. One additional salt bridge, between residues Glu[217]-Lys[329], was also present in over 40% of the converged structures.

Interestingly, the 17-residue linker region between the MA-3 domains (Gly[307]-Pro[323]) was not observed in the electron density maps used to determine the crystal structure of MA-3$_{M-C}$, suggesting that this region is mobile or disordered. This region is included in the structures used as the input for our docking calculations, but is poorly defined in the final set of docked structures (Fig. 3*a*). Although this may reflect the fact that this region is relatively mobile and exists in multiple conformations, it should be noted that no ambiguous interaction restraints, RDC, or torsion angle restraints were included for this region. In a number of the structures the linker region forms part of an additional interface with one of the two MA-3 domains. The possible existence of such transient interactions between the MA-3 domains and the linker region could explain the identification of a number of residues on the surface of the MA-3 domains with shifted NMR signals, which do not appear to form part of the main interdomain interface (Fig. 3). It should also be noted that over half of the residues (Gly[307], Gly[308], Lys[309], Ser[313], Val[314], Gly[316], Ser[317], Gly[319], Gln[322], and Pro[323]) located in this loop showed significant chemical shift changes between the isolated MA-3 domains and the tandem MA-3$_{M-C}$ region (Fig. 2*a*). Although these residues may form additional contacts with the MA-3 domains, we cannot rule out the possibility that these shifts are a result of the differences in mobility and/or the chemical environments of residues located near the termini of the individual MA-3 domains.

Affinity and Stoichiometry of the Pdcd4 MA-3$_{M-C}$·eIF4A Complex—A series of pull-down assays using 7 μM GST-MA-3$_{M-C}$ as bait were performed to investigate the stoichiometry of the MA-3$_{M-C}$·eIF4A complex. Initially, equimolar amounts of MA-3$_{M-C}$ and eIF4A were loaded onto the column. The two proteins co-eluted upon application of buffer containing 10 mM reduced glutathione, as shown in supplemental Fig. S2*a*. The
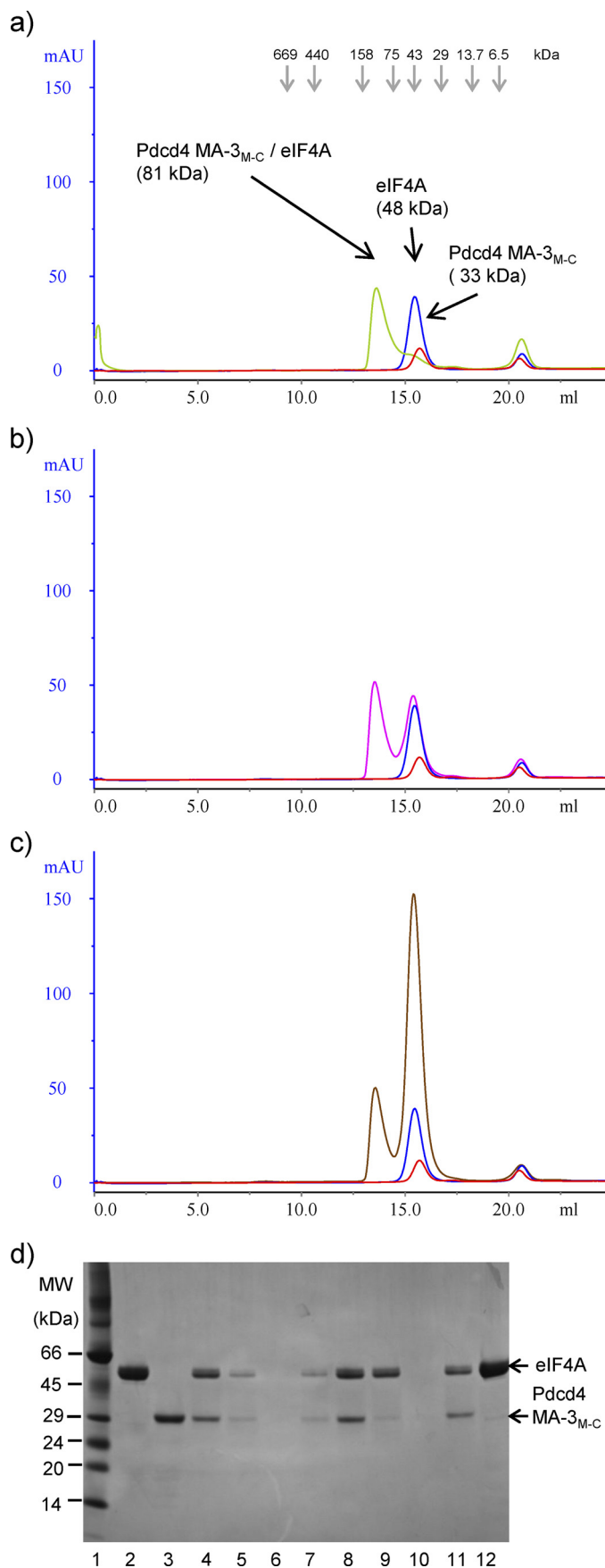
staining intensities observed for the co-eluted GST-MA-3$_{M-C}$ and eIF4A suggests the formation of a tight 1:1 complex. The pulldown experiments were repeated using MA-3$_{M-C}$:eIF4A ratios of 1:3 and 1:5. In both cases an ∼1:1 complex of MA-3$_{M-C}$:eIF4A was co-eluted from the column, with the excess eIF4A coming through in the previous wash fractions (supplemental Fig. S2, *b* and *c*). Comparable results were obtained for pulldown assays between GST full-length Pdcd4 and eIF4A carried out at ratios of 1:1 and 1:3 (data not shown). Pre-equilibration of the GST full-length Pdcd4 fusion protein and eIF4A (at ratios of 1:1 and 1:3) for 30 min at room temperature prior to loading onto the column had no additional effects on binding stoichiometry (data not shown). To further substantiate these findings we carried out a series of analytical gel filtration experiments initially using equimolar amounts (7 μM) of MA-3$_{M-C}$ and eIF4A. The complex eluted at 13.6 ml, which is very close to the expected position for a 1:1 globular complex (13.2 ml) (Fig. 4*a*). To confirm the stoichiometry the eluted complex fractions were analyzed by SDS-PAGE (Fig. 4*d*). Quantification of the relative staining intensity observed for equimolar loads of eIF4A and Pdcd4 MA-3$_{M-C}$ (*lanes 2* and *3*) indicates a 2-fold higher staining intensity for eIF4A. The same relative staining intensity is observed for the gel filtration elution fractions containing the Pdcd4 MA-3$_{M-C}$·eIF4A complex (*lanes 4*, *8*, and *11*), which clearly indicates formation of a 1:1 complex. The experiments were repeated using MA-3$_{M-C}$:eIF4A ratios of 1:2 and 1:5. The gel filtration chromatograms shown in Fig. 4, *b* and *c*, clearly suggest that MA-3$_{M-C}$·eIF4A still form a 1:1 complex, with excess eIF4A eluting as expected for isolated eIF4A, which was confirmed by SDS-PAGE analysis of the fractions (Fig. 4*d*).

The stoichiometry and affinity of Pdcd4 MA-3$_{M-C}$·eIF4A complex formation was further investigated by Biacore experiments conducted at high (150 mM sodium chloride) and low (50 mM sodium chloride) salt concentrations (supplemental Fig. S3). At the lower salt concentration the observed binding of MA-3$_{M-C}$ to eIF4A is consistent with a K_D of 167 nM, whereas at the higher salt concentration a substantially weaker K_D of ∼760 nM was observed. The significant effect of higher ionic strength is not unexpected given the high number of inter-molecular salt bridges and hydrogen bonds observed at the interface of the MA-3$_{M-C}$·eIF4A complex (21, 40). The increase in response units obtained upon binding at the lower salt concentration indicates the formation of a 1:1 complex. The affinity of eIF4A

FIGURE 4. **Gel filtration analysis of the stoichiometry of the Pdcd4 MA-3$_{M-C}$·eIF4A complex.** *Panel a* shows an overlay of typical analytical gel filtration traces obtained for 7 μM samples of MA-3$_{M-C}$ (shown in *red*), eIF4A (*blue*), and a 1:1 mixture of MA-3$_{M-C}$ and eIF4A (*green*). The elution positions of the protein molecular weight standards are indicated *above* the trace. *Panels b* and *c* show typical traces obtained for 1:2 (pink) and 1:5 (brown) mixtures of MA-3$_{M-C}$ (7 μM) and eIF4A, respectively. For comparison the gel filtration traces for 7 μM samples of MA-3$_{M-C}$ (*red*) and eIF4A (*blue*) are also shown. The SDS-PAGE gel in *panel d* shows the analysis of typical elution fractions obtained from the analytical gel filtration experiments. *Lane 1* contains the molecular weight markers, *lanes 2* and *3* are typical eIF4A (7 μM) and MA-3$_{M-C}$ (7 μM) loads, *lanes 4–6* show consecutive elution fractions from the main MA-3$_{M-C}$·eIF4A complex peak (13.6 ml) obtained upon loading a 1:1 mixture of MA-3$_{M-C}$ and eIF4A. Similarly, *lanes 7–8* and *10–11* show consecutive elution fractions from the MA-3$_{M-C}$·eIF4A complex peak (13.6 ml) obtained upon loading a 1:2 and 1:5 mixture of MA-3$_{M-C}$ and eIF4A, respectively. *Lanes 9* and *12* show typical elution fractions from the second peak (15.5 ml) obtained upon loading 1:2 and 1:5 mixtures.
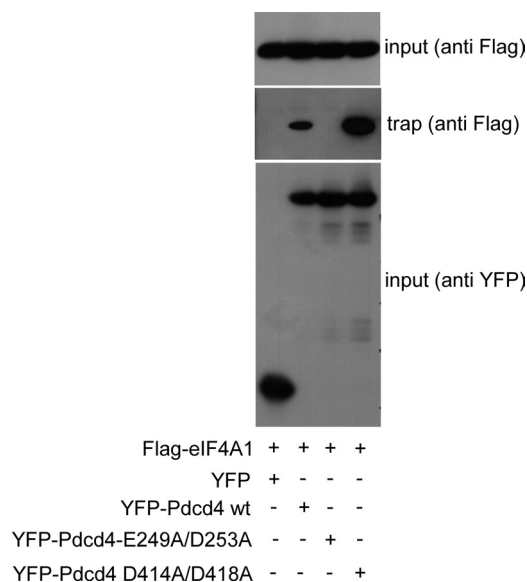
Flag-eIF4A1   +   +   +   +
YFP   +   -   -   -
YFP-Pdcd4 wt   -   +   -   -
YFP-Pdcd4-E249A/D253A   -   -   +   -
YFP-Pdcd4 D414A/D418A   -   -   -   +

FIGURE 5. ***In vivo* interaction of eIF4A with Pdcd4 is mediated via the mode 1 interfaces.** QT6 cells were transfected with the indicated combinations of plasmids encoding FLAG-eIF4A1, YFP, YFP-Pdcd4 wild type, YFP-Pdcd4 E249A/D253A mutant, and YFP-Pdcd4 D414A/D418A mutant. Cells were lysed 24 h post-transfection and the soluble fraction was incubated with GFP-trap beads, resulting in the binding of YFP fusion proteins and their binding partners to the beads. Bound proteins and aliquots of the input extracts were analyzed by Western blotting with antibodies against FLAG and YFP. Although the YFP-Pdcd4 D414A/D418A mutant retained the ability to bind eIF4A, the YFP-Pdcd4 E249A/D253A mutant was not able to bind eIF4A, suggesting that *in vivo* Pdcd4 interacts with eIF4A via the mode 1 interface.

for either full-length Pdcd4 or Pdcd4 MA-3_{M-C} (residues 164–469) has been determined previously by isothermal calorimetry (21, 40). The K_D values obtained in our study appear to be reasonably consistent with the previously reported value of 110 nM for full-length Pdcd4 binding to eIF4A in a 100 mM NaCl, 20 mM Tris, pH 7.6, buffer (21). However, a significantly weaker interaction (K_D = 680 nM) has been reported for eIF4A binding to the tandem MA-3 region of Pdcd4 alone (residues 164–469) in 50 mM NaCl, 25 mM Tris, 7 mM β-mercaptoethanol, pH 7.4, buffer (40).

Characterization of the Mode of Pdcd4-eIF4A Interaction— The *in vitro* experiments clearly indicate the formation of a 1:1 Pdcd4 MA-3_{M-C}·eIF4A complex, with the affinity of the relatively tight interaction showing a significant ionic strength dependence. Previous studies have identified conserved acidic patches on both MA-3 domains that are involved in binding to eIF4A (15, 20–22, 40). To assess the importance of these patches in interactions between full-length Pdcd4 and eIF4A a series of *in vivo* binding experiments were performed. Cells were transfected with expression vectors for YFP fusions of wild type Pdcd4 and two variants containing mutations in the acidic patches of MA-3_M (E249A/D253A) or MA-3_C (D414A/D418A), together with the expression vector for a FLAG-tagged form of eIF4A. Fig. 5 shows the results of Western blot analysis of YFP fusion protein-associated material captured by immobilized GFP-binding protein (49) from a series of transfected cells. The data clearly indicates comparable expression of the wild type and mutant forms of YFP-Pdcd4, however, only mutations within MA-3_M (E249A/D253A) appear to inhibit the interaction with eIF4A, strongly suggesting that MA-3_M contains the

primary binding site for eIF4A *in vivo*. The acidic residues mutated in both MA-3 domains are located on the surface of the proteins and are unlikely to affect the structure of either domain, so the effects observed for MA-3_M are likely to reflect direct changes to the eIF4A binding site (20, 22).

To attempt to further characterize the binding of eIF4A to Pdcd4 MA-3_{M-C} we acquired ^{15}N/^{1}H TROSY spectra from ^{15}N/^{2}H-labeled Pdcd4 MA-3_{M-C} (400 μM) in the presence and absence of equimolar eIF4A, as shown in supplemental Fig. S4. The line widths observed for well resolved peaks that clearly arise from residues within structured regions of Pdcd4 MA-3_{M-C} are consistent with the formation of a relatively tight, 1:1 Pdcd4 MA-3_{M-C}·eIF4A complex (81 kDa). A surprisingly large number of backbone amide peaks appear to have shifted upon binding of eIF4A, however, in addition to perturbations due to direct involvement in the interaction with eIF4A, the binding of eIF4A has recently been shown to induce a significant change in the relative orientation of the two MA-3 domains and loss of the interdomain interface, which will also lead to substantial shifts in signals (21).

*Interaction of Pdcd4 and eIF4Gm—*The previously reported interaction between Pdcd4 and eIF4Gm (14, 39) was investigated by pull-down assays using either GST full-length Pdcd4 or GST-MA-3_{M-C} fusion proteins as bait. In both cases the eIF4Gm eluted in the wash fractions and no interaction with Pdcd4 could be detected (supplemental Fig. S5, *a* and *b*). To assess whether Pdcd4 binds weakly to eIF4Gm (K_D between 10 and 1000 μM), we conducted NMR chemical shift mapping experiments using ^{15}N-labeled full-length Pdcd4 or MA-3_{M-C} and unlabeled eIF4Gm. However, no significant shifts were observed between the NMR spectra of Pdcd4 acquired in the absence and presence of eIF4Gm, as highlighted in supplemental Fig. S5, *panels c* and *d*. Comparable pull-down and chemical shift mapping results were obtained for experiments involving either full-length Pdcd4 or MA-3_{M-C} and the mIF4G domain (data not shown).

DISCUSSION

*Structure of the Pdcd4 MA-3_{M-C} Region and Characterization of Its Interaction with eIF4A—*The NMR data reported here are clearly consistent with the recently reported crystal structure of Pdcd4 MA-3_{M-C} (21), as illustrated by the agreement between the crystal structure and both the NMR mapped interdomain interface and RDC data (Fig. 3 and supplemental Fig. S1*b*). However, comparison of the crystal structure and the NMR-based model produced by HADDOCK (47) suggests that in solution there may be a slight change in the relative orientation of the two MA-3 domains (Fig. 3*b*). Interestingly, the size of the mapped MA-3_M/MA-3_C interface is somewhat larger than the contact surfaces present in the crystal and solution structures (Fig. 3). As previously discussed, some of the additional affected residues may be a result of transient interactions with the linker region. Alternatively, the changes could reflect localized conformational changes induced by the interdomain interaction.

Comparison of the line widths of backbone amide signals in ^{15}N/^{1}H HSQC and ^{15}N/^{13}C/^{1}H HNCO spectra obtained from the isolated MA-3 domains and tandem MA-3_{M-C} region sug-
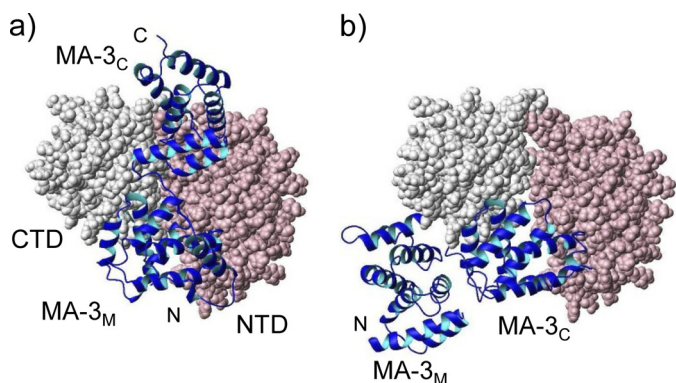
FIGURE 6. **Comparison of Pdcd4 MA-3$_{M-C}$/eIF4A binding modes observed by crystallography.** *Panel a* shows the interaction of MA-3$_{M-C}$ with eIF4A via the mode 1 interaction site (PDB code 3EIQ (21)), with eIF4A shown as a space filled view and MA-3$_{M-C}$ as a *ribbon* representation. The N- and C-terminal domains of eIF4A are colored *pink* and *white*, respectively. The domains of eIF4A, the two MA-3 domains of Pdcd4, and the N and C termini of MA-3$_{M-C}$ are labeled. In this binding mode both MA-3 domains interact with eIF4A. Similarly, *panel b* shows the interaction of MA-3$_{M-C}$ with eIF4A via the mode 2 interaction site. In this binding mode only the MA-3$_C$ domain interacts with eIF4A. As MA-3$_M$ makes no significant contacts with either eIF4A or MA-3$_C$ its relative orientation is dependent on its interaction with a second molecule of eIF4A in the crystal lattice via the mode 1 site. In both binding modes the MA-3 domains bind at the interface between the N- and C-terminal domains of eIF4A, blocking the RNA binding site and preventing the domains from fully closing and forming the active conformation of eIF4A. The eIF4A molecule in *panels a* and *b* are shown in the same orientation.

FIGURE 7. **Potential interactions within a Pdcd4·eIF4A·mIF4G ternary complex.** *Panel a* shows an overlay of the ribbon representation of the backbone topology of yeast eIF4A (PDB code 2VSO (37), shown in *red*) obtained in complex with the mIF4G domain, and human eIF4A (PDB code 3EIQ (21), shown in *blue*) obtained in complex with Pdcd4·MA-3$_{M-C}$. The structures were overlaid on the backbone atoms of residues Phe[24]-Ile[125], Gly[136]-Arg[138], Asp[139]-Leu[223], and Phe[34]-Ile[135], Lys[146]-Gln[148], Ala[151]-Leu[235] of the N-terminal domain of yeast and human eIF4A, respectively. *Panel b* shows a potential model of the relative locations of MA-3$_{M-C}$, eIF4A, and the mIF4G domain in a ternary complex. The structures of eIF4A in complex with the mIF4G domain and MA-3$_{M-C}$ (mode 1 binding) were overlaid as shown in *panel a*. The structures of the mIF4G domain (shown in *red*) and MA-3$_{M-C}$ (*blue*) are shown as ribbon representations of their backbone topologies; whereas the structure of eIF4A obtained in complex with MA-3$_{M-C}$ is shown as a space filled view. For clarity the structure of eIF4A obtained in complex with the mIF4G domain is not shown.

gests there is a degree of motion between the two MA-3 domains (20). In addition, previous NMR binding experiments conducted by Suzuki *et al.* (22) were only able to detect an interaction between the MA-3 domains when covalently linked. These findings are consistent with a somewhat transient interaction between the MA-3 domains, which is only tight enough to be observed when the domains are "tethered" together. This behavior is consistent with the need for the two MA-3 domains to rearrange their relative orientations to bind eIF4A.

Although the solution and crystal structures of MA-3$_{M-C}$ appear to be very similar, our characterization of the stoichiometry and affinity of the MA-3$_{M-C}$·eIF4A complex suggests that some unexpected features of the recently reported structure for the complex, such as the association of two molecules of eIF4A with Pdcd4 MA-3$_{M-C}$, are not preserved under all conditions in solution. In our hands, under near physiological solution conditions MA-3$_{M-C}$ forms a 1:1 complex with eIF4A, according to gel filtration, pull-down, Biacore, and NMR experiments. In addition, our *in vivo* binding experiments show that the acidic patch on MA-3$_M$ forms the major interaction surface with eIF4A *in vivo*, rather than the equivalent site on the C-terminal MA-3 domain. Collectively, these findings strongly suggest that under physiological conditions Pdcd4 and eIF4A form a relatively tight 1:1 complex, which almost certainly corresponds to the recently described crystal structure in which the majority of the contacts are between eIF4A and Pdcd4 MA-3$_M$, including the acidic patch (21, 40). This mode of interaction (mode 1) also featured additional stabilizing interactions between MA-3$_C$ and the C-terminal domain of eIF4A (Fig. 6a), which explains the significantly higher affinity of the tandem MA-3 domains compared with the individual domains (15, 20–22, 40).
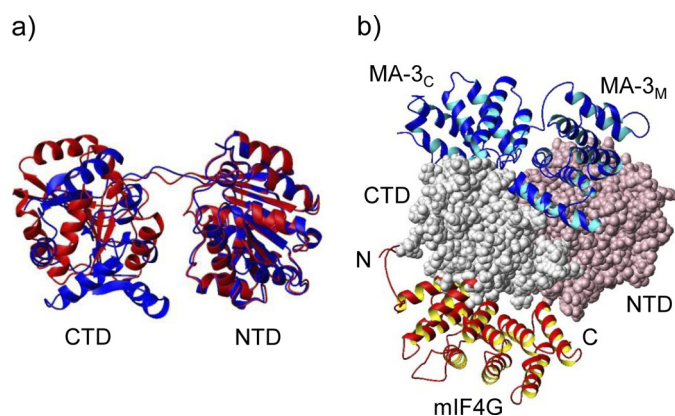
The recently reported crystallographic studies also identified a second mode of Pdcd4-eIF4A interaction (mode 2: Fig. 6b), in which MA-3$_C$ alone contacts eIF4A, making equivalent interactions to those mediated by MA-3$_M$ in the mode 1 complex (21, 40). This second mode of interaction features a significantly reduced contact surface and is likely to be lower affinity. The affinity of the interaction is probably comparable with that seen between the isolated Pdcd4 MA-3$_C$ domain and eIF4A, which reported NMR and isothermal calorimetry studies have shown to be characterized by a dissociation constant of 25–50 μM (20, 21, 40). Consequently, at the concentrations of eIF4A found *in vivo* ($\sim$1 μM) (50), binding of eIF4A at the second low affinity site on Pdcd4 is unlikely to be significant. In agreement with this we found that mutations within the mode 2 binding site on MA-3$_C$ had no discernable effect on eIF4A binding *in vivo*, which suggests that the second mode of interaction is not important under physiological conditions. This gives the potential for the conserved acidic patch on MA-3$_C$ to mediate contacts with other components of the translation initiation complex.

The ability of Pdcd4 to inhibit cap-dependent translation via its interaction with eIF4A is well established, however, a number of important questions relating to its mechanism of action still remain unanswered. Most notably, it has yet to be definitively shown whether Pdcd4 functions by binding to "free" eIF4A and/or eIF4A that has been incorporated into the eIF4F complex. Studies by Yang *et al.* (14) showed that Pdcd4 can inhibit the helicase activity of both free and eIF4F-bound eIF4A. Further *in vitro* studies of the inhibition of cap-dependent translation by Pdcd4, showed that although the addition of purified eIF4F complex resulted in the partial recovery of translation, the addition of free eIF4A had no effect (14). In addition,
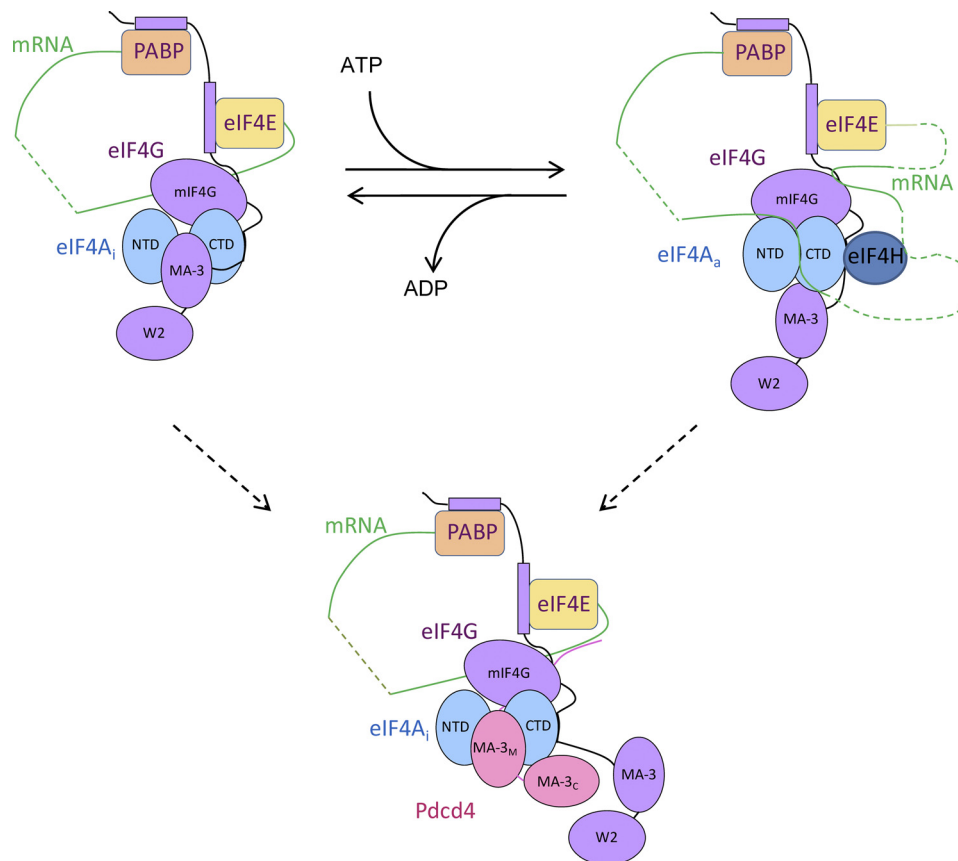
FIGURE 8. **Schematic representation of the proposed mechanism of action of Pdcd4.** The simplified scheme shown is based on the model for the dynamics of the eIF4A/4G/4H complex proposed by Marintchev *et al.* (35). In the absence of nucleotide the interaction between eIF4A and the MA-3 domain of eIF4G stabilizes the inactive open conformation of eIF4A (*eIF4A$_i$*), and at least partially blocks the RNA binding site on eIF4A. In addition, this interaction lowers the affinity of eIF4A for ATP and ADP by ~3-fold thereby favoring the nucleotide-free state of eIF4A. In the presence of ATP, RNA, eIF4Gm, and eIF4H bind cooperatively to eIF4A promoting the closed active conformation (eIF4A$_a$), and stimulating the helicase activity of eIF4A. Pdcd4 has been proposed to function by blocking the RNA-binding site on eIF4A and preventing the conformational change required to form the active conformation, which suggests that the initiation complex containing tightly associated Pdcd4 will be nucleotide free. Additional interactions between Pdcd4 and eIF4Gm may help to trap eIF4A in an inactive conformation, thereby inactivating the entire eIF4F complex.

overexpression of eIF4A was only able to partially relieve the inhibition of the translation of an mRNA with structured 5′ UTR by Pdcd4 *in vivo* (14). These results suggest that Pdcd4 does not simply sequester and/or inhibit free eIF4A, but rather that it binds and inhibits eIF4A molecules that are incorporated into the eIF4F complex.

eIF4A has been shown to interact with both the mIF4G and MA-3 domains of eIF4G leading to some debate as to the number of eIF4A molecules in the eIF4F complex (35, 51–53). Although studies conducted *in vitro* have shown that eIF4G can bind two separate molecules of eIF4A (51, 53), experiments conducted *in vivo* have shown that only one molecule of eIF4A is present in the eIF4F complex (52). In addition, a recent study has reported that the mIF4G and MA-3 domains of eIF4G interact with a single molecule of eIF4A in an anti-cooperative manner (35). The proposed presence *in vivo* of only one molecule of eIF4A in the eIF4F complex is consistent with our detection of only a single high affinity eIF4A binding site on Pdcd4 MA-3$_{M-C}$.

Interaction of Pdcd4 with eIF4Gm—Pdcd4 has been reported to interact with eIF4G. An initial study by Kang *et al.* (39) showed that GST-Pdcd4 was able to pull eIF4G out of HeLa cell extracts. Subsequently, Yang *et al.* (14) performed *in vitro* bind-

ing assays, which showed that Pdcd4 binds specifically to eIF4Gm in both the presence and absence of eIF4A. They also conducted pull-down assays that showed GST-eIF4Gm was able to pull both Pdcd4 and the Pdcd4^{D418A} mutant out of JB6 *p* + cell lysates. It was hypothesized that this interaction was mediated by the MA-3 domains of Pdcd4 (38), however, this claim was challenged by a more recent NMR binding study, which failed to detect any interaction between eIF4Gm and either MA-3$_M$ or MA-3$_C$ (22), and lead to the proposal that the RNA-binding region of Pdcd4 might be responsible for binding eIF4Gm.

We have conducted a series of pull-down and NMR binding experiments using both full-length Pdcd4 and MA-3$_{M-C}$ to detect interactions with either eIF4Gm or the mIF4G domain, but were unable to obtain any evidence of direct binding. The majority of previous pull-down experiments incubated the Pdcd4 or eIF4Gm baits with cell lysates, which may suggest an indirect association as part of a larger, multicomponent complex.

Recently reported gel filtration experiments suggest that Pdcd4, eIF4A, and eIF4Gm can form a relatively tight ternary complex (21). Comparison of the structures obtained for eIF4A in complex with either Pdcd4 MA-3$_{M-C}$ (21, 40) or the mIF4G

domain (37) shows that MA-3$_{M-C}$ and the mIF4G domain bind to distinct surfaces on eIF4A, however, the two domains of eIF4A are orientated differently in each structure (Fig. 7*a*). These differences in orientation are believed to affect the affinity of both proteins for eIF4A, such that Pdcd4 and mIF4G cannot simultaneously bind optimally to eIF4A (21). This is supported by recent work, which showed that the affinity of the interaction of eIF4A with the single MA-3 domain of eIF4G was reduced by at least an order of magnitude in the presence of the mIF4G domain (35).

The question as to whether Pdcd4 simultaneously interacts with both eIF4A and eIF4Gm in the ternary complex has yet to be addressed. In the apparent high affinity interaction between MA-3$_{M-C}$ and eIF4A (mode 1 binding), MA-3$_{M-C}$ and mIF4G would be located on opposite sides of eIF4A and therefore unable to interact, as shown in Fig. 7*b*. However, both the RNA binding region of Pdcd4 and the unstructured regions of eIF4Gm, which are located on either side of the mIF4G domain, are absent from these structures (Fig. 1*c*). If one or both of these regions were involved in binding, this could allow Pdcd4 bound to eIF4A to make favorable interactions with eIF4Gm.

The Role of Pdcd4 in the Inhibition of Cap-dependent Translation—The exact mechanism by which eIF4F stimulates cap-dependent translation has not been elucidated. However, recent work has led to the following model being proposed, (35) as summarized in Fig. 8. In the absence of nucleotide (ATP or ADP) eIF4A interacts with both the mIF4G and MA-3 domains of eIF4G. The interaction with the mIF4G domain appears to be relatively weak, however, the eIF4G MA-3 domain binds tightly to both domains of eIF4A, stabilizing the open inactive conformation and at least partially blocking the RNA binding site. This interaction most probably mimics the mode 2 Pdcd4 MA-3$_{M-C}$-eIF4A interaction seen in the crystal structures (21, 40). In the presence of ATP, the interactions with eIF4G change with the mIF4G domain now contacting both domains of eIF4A stabilizing the closed active conformation. In addition, RNA and either eIF4H or eIF4B also bind cooperatively to the active conformation of eIF4A stimulating cap-dependent translation. In this closed conformation the affinity of the eIF4G MA-3 is weakened, and it is not known whether it remains associated with eIF4A.

It has previously been shown that Pdcd4 competes with the MA-3 domain of eIF4G for binding to eIF4A (14, 15, 21, 22, 38). It seems likely that the two MA-3 domains of Pdcd4 will interact with eIF4A through a larger contact surface and form a tighter interaction than that observed between eIF4A and the single MA-3 domain of eIF4G. In agreement with this hypothesis, the majority of the above mentioned studies suggest that at a 1:1 ratio Pdcd4 can efficiently out-compete eIF4G MA-3 for binding to eIF4A. It therefore seems likely that in the absence of nucleotide, Pdcd4 will bind tightly to eIF4A blocking the RNA-binding site (22) and stabilizing the open, inactive conformation of eIF4A (Fig. 8).

Conclusions—The tumor suppressor protein Pdcd4 inhibits cap-dependent translation by interacting tightly with the RNA helicase eIF4A. As a result mRNAs with structured 5′ UTRs, such as growth factors and oncogenes, are particularly susceptible to translational inhibition by Pdcd4. The work reported in this article suggests that the tandem MA-3 region of Pdcd4 forms a functionally relevant 1:1 complex with eIF4A, blocking the RNA binding site on eIF4A and holding eIF4A in an inactive conformation. Pdcd4 has previously been reported to interact with eIF4Gm, however, we were unable to observe any direct interaction, which suggests either an indirect association, or stabilization of direct contacts, as part of a larger functional complex.

REFERENCES

1. Shibahara, K., Asano, M., Ishida, Y., Aoki, T., Koike, T., and Honjo, T. (1995) *Gene* **166,** 297–301
2. Cmarik, J. L., Min, H., Hegamyer, G., Zhan, S., Kulesz-Martin, M., Yoshinaga, H., Matsuhashi, S., and Colburn, N. H. (1999) *Proc. Natl. Acad. Sci. U.S.A.* **96,** 14037–14042
3. Jansen, A. P., Camalier, C. E., and Colburn, N. H. (2005) *Cancer Res.* **65,** 6034–6041
4. Hilliard, A., Hilliard, B., Zheng, S. J., Sun, H., Miwa, T., Song, W., Göke, R., and Chen, Y. H. (2006) *J. Immunol.* **177,** 8095–8102
5. Afonja, O., Juste, D., Das, S., Matsuhashi, S., and Samuels, H. H. (2004) *Oncogene* **23,** 8135–8145
6. Chen, Y., Knösel, T., Kristiansen, G., Pietas, A., Garber, M. E., Matsuhashi, S., Ozaki, I., and Petersen, I. (2003) *J. Pathol.* **200,** 640–646
7. Wang, Q., Sun, Z., and Yang, H. S. (2008) *Oncogene* **27,** 1527–1535
8. Wang, X., Wei, Z., Gao, F., Zhang, X., Zhou, C., Zhu, F., Wang, Q., Gao, Q., Ma, C., Sun, W., Kong, B., and Zhang, L. (2008) *Anticancer Res.* **28,** 2991–2996
9. Zhang, H., Ozaki, I., Mizuta, T., Hamajima, H., Yasutake, T., Eguchi, Y., Ideguchi, H., Yamamoto, K., and Matsuhashi, S. (2006) *Oncogene* **25,** 6101–6112
10. Jansen, A. P., Camalier, C. E., Stark, C., and Colburn, N. H. (2004) *Mol. Cancer Ther.* **3,** 103–110
11. Mudduluru, G., Medved, F., Grobholz, R., Jost, C., Gruber, A., Leupold, J. H., Post, S., Jansen, A., Colburn, N. H., and Allgayer, H. (2007) *Cancer* **110,** 1697–1707
12. Bitomsky, N., Wethkamp, N., Marikkannu, R., and Klempnauer, K. H. (2008) *Oncogene* **27,** 4820–4829
13. Singh, P., Marikkannu, R., Bitomsky, N., and Klempnauer, K. H. (2009) *Oncogene* **28,** 3758–3764
14. Yang, H. S., Jansen, A. P., Komar, A. A., Zheng, X., Merrick, W. C., Costes, S., Lockett, S. J., Sonenberg, N., and Colburn, N. H. (2003) *Mol. Cell. Biol.* **23,** 26–37
15. Yang, H. S., Cho, M. H., Zakowicz, H., Hegamyer, G., Sonenberg, N., and Colburn, N. H. (2004) *Mol. Cell. Biol.* **24,** 3894–3906
16. Bitomsky, N., Böhm, M., and Klempnauer, K. H. (2004) *Oncogene* **23,** 7484–7493
17. Wedeken, L., Ohnheiser, J., Hirschi, B., Wethkamp, N., and Klempnauer, K. H. (2010) *Genes and Cancer* **1,** 293–301
18. Böhm, M., Sawicka, K., Siebrasse, J. P., Brehmer-Fastnacht, A., Peters, R., and Klempnauer, K. H. (2003) *Oncogene* **22,** 4905–4910
19. Lankat-Buttgereit, B., and Göke, R. (2009) *Biol. Cell* **101,** 309–317
20. Waters, L. C., Veverka, V., Böhm, M., Schmedt, T., Choong, P. T., Muskett, F. W., Klempnauer, K. H., and Carr, M. D. (2007) *Oncogene* **26,** 4941–4950
21. Loh, P. G., Yang, H. S., Walsh, M. A., Wang, Q., Wang, X., Cheng, Z., Liu, D., and Song, H. (2009) *EMBO J.* **28,** 274–285
22. Suzuki, C., Garces, R. G., Edmonds, K. A., Hiller, S., Hyberts, S. G., Marintchev, A., and Wagner, G. (2008) *Proc. Natl. Acad. Sci. U.S.A.* **105,** 3274–3279
23. Ponting, C. P. (2000) *Trends Biochem. Sci.* **25,** 423–426
24. Marintchev, A., and Wagner, G. (2004) *Q. Rev. Biophys.* **37,** 197–284
25. Pestova, T. V., Lorsch, J. R., and Hellen, C. U. T. (2007) in *Translational Control in Biology and Medicine* (Mathews, M. B., Sonenberg, N., and Hershey, J. W. B., eds) pp 87–128, Cold Spring Harbor Laboratory Press, Cold Spring Harbor, NY
26. Abramson, R. D., Dever, T. E., Lawson, T. G., Ray, B. K., Thach, R. E., and

Merrick, W. C. (1987) *J. Biol. Chem.* **262,** 3826 – 3832

27. Richter-Cook, N. J., Dever, T. E., Hensold, J. O., and Merrick, W. C. (1998) *J. Biol. Chem.* **273,** 7579 – 7587

28. Rogers, G. W., Jr., Richter, N. J., Lima, W. F., and Merrick, W. C. (2001) *J. Biol. Chem.* **276,** 30914 – 30922

29. Rozen, F., Edery, I., Meerovitch, K., Dever, T. E., Merrick, W. C., and Sonenberg, N. (1990) *Mol. Cell. Biol.* **10,** 1134 – 1144

30. Marcotrigiano, J., Lomakin, I. B., Sonenberg, N., Pestova, T. V., Hellen, C. U., and Burley, S. K. (2001) *Mol. Cell* **7,** 193 – 203

31. Lamphear, B. J., Kirchweger, R., Skern, T., and Rhoads, R. E. (1995) *J. Biol. Chem.* **270,** 21975 – 21983

32. Morino, S., Imataka, H., Svitkin, Y. V., Pestova, T. V., and Sonenberg, N. (2000) *Mol. Cell. Biol.* **20,** 468 – 477

33. Imataka, H., and Sonenberg, N. (1997) *Mol. Cell. Biol.* **17,** 6940 – 6947

34. De Gregorio, E., Preiss, T., and Hentze, M. W. (1999) *EMBO J.* **18,** 4865 – 4874

35. Marintchev, A., Edmonds, K. A., Marintcheva, B., Hendrickson, E., Oberer, M., Suzuki, C., Herdy, B., Sonenberg, N., and Wagner, G. (2009) *Cell* **136,** 447 – 460

36. Oberer, M., Marintchev, A., and Wagner, G. (2005) *Genes Dev.* **19,** 2212 – 2223

37. Schütz, P., Bumann, M., Oberholzer, A. E., Bieniossek, C., Trachsel, H., Altmann, M., and Baumann, U. (2008) *Proc. Natl. Acad. Sci. U.S.A.* **105,** 9564 – 9569

38. LaRonde-LeBlanc, N., Santhanam, A. N., Baker, A. R., Wlodawer, A., and Colburn, N. H. (2007) *Mol. Cell. Biol.* **27,** 147 – 156

39. Kang, M. J., Ahn, H. S., Lee, J. Y., Matsuhashi, S., and Park, W. Y. (2002) *Biochem. Biophys. Res. Commun.* **293,** 617 – 621

40. Chang, J. H., Cho, Y. H., Sohn, S. Y., Choi, J. M., Kim, A., Kim, Y. C., Jang, S. K., and Cho, Y. (2009) *Proc. Natl. Acad. Sci. U.S.A.* **106,** 3148 – 3153

41. Waters, L. C., Böhm, M., Veverka, V., Muskett, F. W., Frenkiel, T. A., Kelly, G. P., Prescott, A., Dosanjh, N. S., Klempnauer, K. H., and Carr, M. D. (2006) *J. Biomol. NMR* **36,** 18 – 18

42. Waters, L. C., Oka, O., Muskett, F. W., Strong, S. L., Schmedt, T., Klempnauer, K. H., and Carr, M. D. (2010) *Biomol. NMR Assign.* **4,** 49 – 53

43. Waters, L., Yue, B., Veverka, V., Renshaw, P., Bramham, J., Matsuda, S., Frenkiel, T., Kelly, G., Muskett, F., Carr, M., and Heery, D. M. (2006) *J. Biol. Chem.* **281,** 14787 – 14795

44. Renshaw, P. S., Panagiotidou, P., Whelan, A., Gordon, S. V., Hewinson, R. G., Williamson, R. A., and Carr, M. D. (2002) *J. Biol. Chem.* **277,** 21598 – 21603

45. Boozer, C., Kim, G., Cong, S., Guan, H., and Londergan, T. (2006) *Curr. Opin. Biotechnol.* **17,** 400 – 405

46. Homola, J. (2008) *Chem. Rev.* **108,** 462 – 493

47. Dominguez, C., Boelens, R., and Bonvin, A. M. (2003) *J. Am. Chem. Soc.* **125,** 1731 – 1737

48. Cornilescu, G., Delaglio, F., and Bax, A. (1999) *J. Biomol. NMR* **13,** 289 – 302

49. Rothbauer, U., Zolghadr, K., Muyldermans, S., Schepers, A., Cardoso, M. C., and Leonhardt, H. (2008) *Mol. Cell. Proteomics* **7,** 282 – 289

50. Pause, A., Méthot, N., Svitkin, Y., Merrick, W. C., and Sonenberg, N. (1994) *EMBO J.* **13,** 1205 – 1215

51. Korneeva, N. L., Lamphear, B. J., Hennigan, F. L., Merrick, W. C., and Rhoads, R. E. (2001) *J. Biol. Chem.* **276,** 2872 – 2879

52. Li, W., Belsham, G. J., and Proud, C. G. (2001) *J. Biol. Chem.* **276,** 29111 – 29115

53. Nielsen, K. H., Behrens, M. A., He, Y., Oliveira, C. L., Sottrup Jensen, L., Hoffmann, S. V., Pedersen, J. S., and Andersen, G. R. (2011) *Nucleic Acids Res.,* in press